Published in final edited form as:

Vision Res. 2014 October ; 103: 49–62. doi:10.1016/j.visres.2014.07.020.

Pharmacological inhibitions of glutamate transporters EAAT1 and EAAT2 compromise glutamate transport in photoreceptor to ON- bipolar cell synapses

Dennis Y. Tse[1], **Inyoung Chung**[1,2], and **Samuel M. Wu**[1]

[1]Cullen Eye Institute, Department of Ophthalmology, Baylor College of Medicine, Houston, Texas, USA

[2]Department of Ophthalmology, Gyeongsang National University, Jinju, Republic of Korea

Abstract

To maintain reliable signal transmission across a synapse, free synaptic neurotransmitters must be removed from the cleft in a timely manner. In the first visual synapse, this critical task is mainly undertaken by glutamate transporters (EAATs). Here we study the differential roles of the EAAT1, EAAT2 and EAAT5 subtypes in glutamate (GLU) uptake at the photoreceptor-to-depolarizing bipolar cell synapse in intact dark-adapted retina. Various doses of EAAT blockers and/or GLU were injected into the eye before the electroretinogram (ERG) was measured. Their effectiveness and potency in inhibiting the ERG b-wave were studied to determine their relative contributions to the GLU clearing activity at the synapse. The results showed that EAAT1 and EAAT2 plays different roles. Selectively blocking glial EAAT1 alone using UCPH101 inhibited the b-wave 2–24 hours following injection, suggesting a dominating role of EAAT1 in the overall GLU clearing capacity in the synaptic cleft. Selectively blocking EAAT2 on photoreceptor terminals had no significant effect on the b-wave, but increased the potency of exogenous GLU in inhibiting the b-wave. These suggest that EAAT2 play a secondary yet significant role in the GLU reuptake activity at the rod and the cone output synapses. Additionally, we have verified our electrophysiological findings with double-label immunohistochemistry, and extend the literature on the spatial distribution of EAAT2 splice variants in the mouse retina.

Correspondence: Dennis Y. Tse, PhD., *Department of Ophthalmology* Baylor College of Medicine, One Baylor Plaza, NC-205, Houston, TX 77030, Tel: (713) 798-5966, Fax: (713) 798-6457, Work ytse@bcm.edu, Permanent dentse@gmail.com.
†The first two authors are co-first authors

The manuscript is submitted together with a companion paper titled: *Possible Roles of Glutamate Transporter EAAT5 in Mouse Cone Depolarizing Bipolar Cell Light Responses*.

DISCLOSURES

No conflicts of interest, financial or otherwise, are declared by the authors.

AUTHOR CONTRIBUTIONS

D.Y.T and I.C. participated in designing the experiment, collecting and analyzing the data, and writing the article. S.M.W. was involved in designing the experiment, interpreting the data, and writing the article.

Keywords

Retina; EAAT1; EAAT2; GLT1; electroretinogram; immunohistochemistry

1. INTRODUCTION

Glutamate is the neurotransmitter used by the first synapse in the retina (Massey and Redburn 1987; Copenhagen and Jahr 1989; Massey 1990). L-glutamate (GLU) is tonically released at a high rate in the dark by photoreceptors (Dowling and Ripps 1973; Copenhagen and Jahr 1989) and activates postsynaptic receptors on second-order neurons. Photoreceptors hyperpolarize in light (Baylor and Fuortes 1970), resulting in decreased vesicular GLU release, which modulates synaptic input to bipolar and horizontal cells (Cervetto and MacNichol 1972; Murakami, Otsuka et al. 1975; Attwell 1990).

To ensure reliable signal transmission, synaptic GLU concentration must be regulated by quick removal of free GLU from the cleft. This is the classical role of excitatory amino acid transporters (EAATs), and is a two-step process. The transport turnover rate for GLU of the EAATs was found to be very slow (Wadiche, Arriza et al. 1995), but the EAATs have high affinity to GLU (Diamond and Jahr 1997) and are present at presynaptic terminals at high-density (Hasegawa, Obara et al. 2006). Therefore, it is suggested that they clear free synaptic GLU in a way resembling a buffer (Tong and Jahr 1994) instead of just a transporter. In the retina, glutamate not reabsorbed by the presynaptic EAATs is thought to be removed and recycled through a secondary process, which involves transporting into the Muller cell via its membrane EAAT1 and conversion into glutamine before transporting back to the photoreceptors (Hertz, Dringen et al. 1999).

To date, five subtypes of EAATs have been identified in the mammalian central nervous system (Danbolt 2001; Shigeri, Seal et al. 2004), namely EAAT1 to EAAT5. In retina, EAAT1 has been found on Müller cells in rat (Rauen, Rothstein et al. 1996). EAAT2, also named GLT1, was found on rod and cone terminals in rat (Rauen and Kanner 1994) and mouse (Haverkamp and Wassle 2000), but surprisingly not in mammalian Müller cells. GLT1 was further characterized as splice variants GLT1A, located in rod spherules, and GLT1B, in cone pedicles and some bipolar cells in rat (Reye, Sullivan et al. 2002). EAAT3 was found to be present on the horizontal cells, amacrine cells and ganglion cells in the rat (Rauen, Rothstein et al. 1996; Schultz and Stell 1996). EAAT4 was found to be present on the Müller cells and astrocytes in rat retina (Ward, Jobling et al. 2004). EAAT5 has been shown to be present on presynaptic rod terminals in the mouse (Hasegawa, Obara et al. 2006; Wersinger, Schwab et al. 2006).

The objectives of the present study are to determine the differential roles of EAAT2, EAAT1 and EAAT5 in the signal inputs of depolarizing retinal bipolar cells (DBCs). The primary research hypothesis is that the above EAATs are responsible for the uptake/binding of free synaptic GLU in the outer plexiform layer and that pharmacologically inhibiting them would disrupt signal transmission between the photoreceptors and DBCs. Several specific and non-specific EAAT blockers are injected and their potencies in inhibiting the

ERG b-wave (which originates from DBCs) were studied in intact dark-adapted mouse retina.

Our baseline data showed that the synthetic glutamate analogue (LAP4) was more potent than GLU in inhibiting the ERG b-wave when injected intravitreally. There is a possibility that the difference in their potencies was because extracellular free GLU but not LAP4 was being removed by EAATs at the photoreceptor-to-DBC synapses. Therefore, our research hypothesis is that the effect of extracellular GLU in saturating DBC signal transmission is influenced by the GLU clearing activities of EAATs. GLU was co-injected with EAAT blockers and the altered GLU potency in inhibiting the ERG b-wave was determined in intact dark-adapted retina.

The measured potencies of injected EAAT blockers and GLU under different conditions have shed light on the GLU clearing functions of various EAATs on the endogenous synaptic glutamate equilibrium. That was achieved by taking advantage of an infrared guided drug injection system and ERG recording techniques in total darkness. Such an approach is advantageous over others because it is more physiological as all in-vivo fluid flow and transporter systems in the eye are intact and functional. Also, the synaptically released glutamate would not be washed out by the perfused buffer as reported under in-vitro conditions (Winkler, Kapousta-Bruneau et al. 1999), and any possible confounding global side-effects from permanently knocking out the EAATs (Rothstein, Dykes-Hoberg et al. 1996; Tanaka, Watase et al. 1997; Watase, Hashimoto et al. 1998) could be avoided. In the second half of the study, we have confirmed our electrophysiological findings by double immunohistochemistry staining and extended the literature on the spatial distribution of EAAT2 splice variants in the mouse retina.

2 MATERIALS AND METHODS

2.1 Animals

One hundred and twenty-three Wildtype mice (C57BL/6) from Jackson Laboratories (Bar Harbor, ME) between 8 and 12 weeks old were used for experiments. Animals were treated in accordance with NIH guidelines and the Baylor College of Medicine IACUC welfare guidelines which complied with The Code of Ethics of the World Medical Association (Declaration of Helsinki) for experiments involving humans.

2.2 Intravitreal Injection

Solutions containing glutamate (Cat. no. g1626, Sigma-Aldrich, St. Louis, MO), LAP4 (Cat. no. 0103, Tocris bioscience, Minneapolis, MN), Dihydrokainic acid (Cat. no.0111, Tocris bioscience) or TBOA (Cat. no. 1223, Tocris bioscience) were prepared by dissolving in sterile Balanced Salt Solution (Alcon, Fort Worth, TX). Solution containing UCPH (Cat. no. 3490, Tocris bioscience) was prepared by dissolving in Dimethyl sulfoxide (DMSO, Sigma-Aldrich). Unless otherwise stated, drug concentrations presented in the results were vitreal/retinal concentrations calculated assuming that the injected solution was diluted by 20 μL of vitreous (Saszik, Robson et al. 2002; Gao, Pennesi et al. 2006).

Mice were first dark-adapted for a minimum of 2 hours. Prior to intra-vitreal injection, mice were anaesthetized with weight-based intraperitoneal injection of solution containing ketamine (46mg/ml), xylazine (9.2mg/ml), and acepromazine (0.77mg/ml). After that, a single drop of 0.5% proparacaine hydrochloride, 1% tropicamide, and 2.5% phenylephrine was applied on the cornea for topical anesthesia and pupil mydriasis under dim red light. The injection procedure was performed under infrared illumination. First, a 32-gauge disposable needle was used to puncture the eye at the pars planar. Solutions containing the drug or the control were then injected in one eye using a NanoFil microinjection system (World Precision Instrument, FL) into the vitreous chamber through the puncture with a 34-gauge blunt needle visible behind the dilated pupil. The needle was allowed to stay for an additional 30sec in the eye after the injection to avoid any injected drug from escaping the eye when the needle was withdrawn. The volume of fluid injected was 1 μL for saline based drug, or 0.2 μL for DMSO based drug.

2.3 Electroretinogram

Immediately after intravitreal injection, mice were placed on a stereotaxic platform with their body temperature maintained at 39°C using a heating pad. Reference and ground electrodes were placed in the forehead and tail, respectively. A blunt platinum needle active electrode was placed in contact with the center of each cornea. Then a drop of methylcellulose gel (2.5%) was applied to the eye. The platform was then placed inside a Ganzfeld dome coated with highly reflective white paint (Munsell Paint, New Windsor, NY) and the mice were then allowed to remain in complete darkness for 3 min before recording.

All scotopic stimuli were generated using light emitting diodes as half millisecond square pulse of 505 nm peak wavelength. A scotopic ERG protocol comprised of progressively increasing stimuli strength was implemented to measure a- and b- waves in different zones as defined previously (Abd-El-Barr, Pennesi et al. 2009) to facilitate dissection of the rod and cone pathways. Saturating stimuli were generated with 1500 W xenon flash bulbs (Novatron, Dallas, TX) and attenuated with apertures and diffusers at the end of the scotopic protocol. All flashes were calibrated with a photometer (ILT1700 International Light, MA) and converted to the unit photoisomerizations/rod (R*/Rod), where 1 scot cd m2 = 581 photoisomerization/rod/s (Saszik, Robson et al. 2002; Lyubarsky, Daniele et al. 2004). To study the time course for the effect of the injected drugs, the above protocol, which lasted 11 min, was implemented 4 times in the first hours following the injection.

ERG signals were amplified using Grass P122 amplifiers (band-pass 0.1 to 1,000Hz; Grass Instruments, West Warwick, RI) and then acquired at a sampling rate of 10 kHz with a data acquisition board (USB-6216, National Instruments, TX). Signal averaging was employed to increase the signal-to-noise ratio of recorded ERG using custom codes written in Matlab (The MathWorks, Natick, MA). 25 responses were averaged with an interval of 2 sec between each flash at the lowest intensity. Fewer responses were averaged with a longer interval between flashes as the intensity of the flash increased. The scotopic b-wave was digitally filtered using the “filtfilt” function (low-pass filtered; F_c = 60 Hz) in Matlab to remove oscillatory potentials before fitting. Dose-response curves showing the amplitude of b-wave against drug concentration were fitted using the DoseRep function of OriginPro v8.6

(OriginLab Corp., Northampton, MA) pharmacology toolbox. Statistical comparison between groups in this study was calculated using unpaired t-test, or one-way ANOVA with Tukey post-hoc analysis. Significant difference was defined as $p<0.05$ unless otherwise stated. ERG data presented in this report are normalized to compensate for the effect from injecting the solvents (described in detail in section 3.1 of the companion paper). For example, the normalized b-wave amplitude for the GLU injected group was calculated using the Equation 1 below:

$$normalized\ amplitude_{GLU} = \frac{amplitude_{GLU\ injected\ eye}}{amplitude_{uninjected\ fellow\ eye}} X \frac{Mean\ amplitude_{uninjected\ control\ eyes}}{Mean\ amplitude_{saline\ injected\ eyes}}$$

2.4 Antibody Characterization

The following antibodies were acquired from commercial suppliers for labeling specific cell types of the retina (Table 1). Horizontal cells were immuno-labeled with a mouse monoclonal antibody against calbindin (de Melo, Qiu et al. 2003). Anti-GLT1A and Anti-GLT1B antisera were purchased from LifeSpan Bioscience (Seattle, WA) and Abcam plc (Cambridge, MA), respectively. The antiserum has been shown to label neurons in the CA1 region of the rat hippocampus (Rose, Koo et al. 2009). ON-cone bipolar cells and rod bipolar cells were immuno-stained with a mouse monoclonal or a rabbit polyclonal antibody against G-protein Goα (Haverkamp and Wassle 2000). Rod bipolar cells were immuno-labeled with rabbit and mouse antibodies against PKCα (Zhang, Yang et al. 2005). Rod photoreceptor spherules were labeled with anti-PSD95 antibody (Oh, Khan et al. 2007). Fluorescein tagged peanut agglutinin (PNA) was used to stain cone pedicles (Blanks and Johnson 1983).

2.5 Tissue preparation and immunohistochemistry

Mice were deeply anaesthetized when the eyes were enucleated, and then immediately euthanized by an overdose of anesthesia. The eyes were then dissected carefully to isolate whole retina, which was subsequently fixed in 4% paraformaldehyde (Electron Microscopy Science, Fort Washington, PA) in phosphate buffer (DPBS, Invitrogen, La Jolla, CA), pH 7.4, at room temperature for 45 minutes. IHC was performed using an indirect antibody method. Retinae were cut into vertical sections 40μm in thickness using a vibratome. Sections were dephosphorylated by incubating overnight with alkaline phosphatase as described previously (Reye, Sullivan et al. 2002), and subsequently blocked with 10% donkey serum (Jackson Immunoresearch, West Grove, PA) in TBS (DPBS with 0.5% Triton X-100 (Sigma) and 0.1% sodium azide (Sigma), pH 7.2) at 4°C overnight to decrease nonspecific labeling.

The free-floating sections were incubated with primary antibodies at 4°C for 4 days in the presence of 3% donkey serum-TBS. Controls lacking primary antibodies were also processed. After several rinses, the sections were transferred and incubated overnight in 3% normal donkey serum-TBS solution containing donkey-hosted secondary antibodies conjugated with Cy5, Cy3 (1:200, Jackson Immunoresearch), or Alexa Fluor 488 (1:200, Molecular Probes, Eugene, OR) at 4°C. After rinsing several times, the sections were

mounted with Vectashield medium (Vector Laboratories, Burlingame, CA) and coverslipped before being observed with a confocal laser scanning microscope (LSM 510; Zeiss, Thornwood, NY). Images were acquired using 40× and 63× oil-immersion objectives with Zeiss LSM software. Adobe Photoshop CS5 (Adobe Systems, San Jose, CA) was then used to crop images and uniformly apply identical brightness and contrast adjustments.

3 RESULTS

3.1 Effects of exogenous glutamate on ERG in dark-adapted living mouse eyes

To establish the baseline potency of injected glutamate in inhibiting signal transmission, GLU was dissolved in saline and injected into the eyes of 30 mice. It was found that the exogenously introduced neurotransmitter inhibited the ERG b-wave (which originates from DBCs) shortly after its introduction. As shown in Fig. 1A, b-wave was inhibited the most at the 5 min post-injection time point and then recovered gradually during the 1 hour window for all stimulus strengths. Using the baseline data established in section 3.1 of the companion paper, the present results are normalized according to their corresponding stimulus strength and recorded time to compensate for artifactual effects of puncturing the eye and injecting saline. For example, amplitudes of the ERG in GLU injected eyes were normalized using Equation 1 in the method section 2.3.

The dose-response relationship between GLU concentration and b-wave amplitude was then determined using a titrating experimental approach, in which various concentrations of GLU were injected before ERG was measured. The data at the 5 min time point was chosen, when the inhibition was maximum, for the above purpose. Figure 1B illustrates the residual b-wave amplitude against stimulus strength after injecting various concentrations of GLU. To facilitate dissection of the rod/cone pathways the stimulus strength is divided into four different zones (Abd-El-Barr, Pennesi et al. 2009), which correspond to the operating ranges of different retinal neurons including rod, cone, DBC_R, DBC_C and AII amacrine cells (Fig. 1C). For simplicity, zones I and II together may be regarded as scotopic zones, while zone III and IV may be respectively regarded as mesopic and photopic. Full inhibition of the b-wave was observed when measured with a zone III moderate stimulus but not with a weaker zone II or a stronger zone IV stimulus. The b-wave in zone III is most susceptible to the inhibition by exogenous GLU.

The amplitude of the b-wave is then normalized and plotted against the retinal concentration of GLU in Fig. 2A–C at three different representative stimulus strengths. As read from the drop-lines, GLU has IC50 values of 4.47, 3.58 and 4.21 log μM (or 29 mM, 3.8 mM and 16 mM in linear scale) at stimulus strengths of 6.2, 1.8 and 0.1 log R*/Rod, respectively. Corresponding IC50 values for LAP4 tested under the same conditions were 1.57, 0.32 and 0.65 log μM (37, 2.1 and 4.5 μM), as described in section 3.2 of the companion paper. The IC50 values are defined as the concentration of a molecule that inhibits 50% of the measured response. The fact that $IC50_{GLU}$S were higher than $IC50_{LAP4}$S suggests that GLU is less potent than LAP4 on inhibiting the b-wave.

There is no evidence that the GLU dose-dependent inhibition of b-wave was caused by a suppressed phototransduction. GLU inhibited the b-wave without systematically affecting

the a-wave. As shown in Fig. 2D, E, increasing the concentration of GLU produced more variation but not a stronger or a systematic inhibition on the amplitude of a-wave. Because a-waves normally manifest as a PIII component truncated by a PII component (Granit 1933), it is likely that GLU increased the variation of the a-wave through suppressing the b-wave.

3.2 Effects of EAAT2 and EAAT1 blockers on ERG

To determine the role of EAAT2 and EAAT1 on the uptake of endogenous synaptic GLU, their blockers were injected into the mouse eye. Injected EAAT2 specific blocker dihydrokainic acid (130-fold selective for EAAT2 over EAAT1) partially inhibited the b-wave only when its concentration was high (Fig. 3A, B). The time course of inhibition differed depending on the stimulus strength (Fig. 3A). For stimuli of 0.6 log R*/Rod or stronger, b-wave amplitudes decreased with time and were the lowest at the 50 min point. For stimuli of 0.1 log R*/rod or weaker, b-wave amplitudes were the lowest at the beginning and increased over the 50 min period measured. The inhibitory effects of dihydrokainic acid (DHK) on the b-wave were studied using a titrating experimental approach to establish the dose-response relationship. Twenty-six mice were injected with various concentrations of DHK and then ERG was used to monitor its effect on retinal functions. Data from the time point when inhibitions were at maximum were chosen for plotting the dose-response curves in Fig. 3C–E, at three stimulus strengths. DHK has IC50 values of 4.02, 4.30 and 4.67 log μM (10, 20 and 47 mM in linear scale) at stimulus strengths of 6.2, 1.8 and 0.1 log R*/rod, respectively. It partially inhibited amplitudes of the b-wave by 39%, 40% and 62% respectively at the above stimulus strengths.

DHK had little effect on the amplitude of the a-wave and had a minor effect on increasing the latency of a-wave when it inhibited the b-wave, as illustrated in the representative raw ERG traces in Fig. 4A. Such effects were not so dose-dependent (Fig. 4B,C).

Six mice were injected with UCPH (a potent selective EAAT1 blocker) of 400 μM retinal concentration in one eye, while another six mice were injected with the solvent DMSO. It was found that amplitudes of the b-wave were partially inhibited by UCPH, and that the inhibition developed slowly in the first 24 hours after injection and recovered significantly after another 9 days (Fig. 5A). Inhibition was not observed during the first hour. Minor inhibition was detected 2 hours after injection. At the 24^{th} hour, injected eyes have mean b-wave inhibited by 41–27% relative to the fellow eye. UCPH produced 14–30% significantly stronger inhibitions than those of the DMSO. Inhibition was most prominent in zone II. There were no significant differences between UCPH and DMSO injected eyes in the amplitudes of the a-wave. Higher retinal concentration of UCPH was not tested because of the limited solubility of UCPH in DMSO, and the limited volume of DMSO that can be injected into the eye without affecting the b-wave.

3.3 Effects of co-injecting EAAT inhibitors and glutamate

To study the contribution of EAAT2 to the glutamate clearing activity in the photoreceptor-DBC synapse, glutamate (GLU) was co-injected with a threshold retinal concentration (200 μM or 2.3 log μM) of DHK. According to our earlier data (Fig. 3B–E), this concentration of

DHK inhibited amplitudes of the b-wave by 10% to 23% at the 5 min time point depending on the stimulus strength.

The above paradigm was repeated in another group of mice using a threshold retinal concentration (0.5 μM or −0.3 log μM) of TBOA, which is a non-specific EAAT blocker commonly used to study the effect of blocking EAAT5. In section 3.3 of our companion paper, we have shown that TBOA inhibited the ERG b-wave in a dose-dependent manner similar to that of GLU or TBOA. The above threshold concentration of TBOA was found to inhibit the amplitude of the b-wave by 16% to 23% at various stimulus levels. The dose-response curves for GLU in the presence of DHK or TBOA (Fig. 6) were tested and modeled under the conditions described above. To isolate the effect of GLU, data were normalized to compensate for the minor inhibitory effects of DHK or TBOA with the following sample Equation 2:

$$normalized\,b-wave_{GLU,DHK}=\frac{B-wave_{GLU,DHK}}{B-wave_{uninjected\ fellow\ eye}}X\frac{MeanB-wave_{uninjected\ control\ eyes}}{MeanB-wave_{200\mu MDHK}}$$

As shown in Fig. 1B and 2A–C, intravitreally injected GLU produced the most inhibition of the b-wave measured with a zone III stimulus of log 1.8 R*/Rod, and lesser percentages of inhibition when measured with a weaker or a stronger stimuli. This inhibitory pattern was preserved when GLU was co-injected with either DHK or TBOA. The IC50 values for GLU were, however, quite different between mice injected with the two EAAT inhibitors. Under the strongest stimulus GLU had a lower value of 1.95 log μM (92 μM) in the presence of DHK compared to the higher value of 4.25 log μM (18 mM) in the presence of TBOA (Fig. 6A, B). The difference was 2.3 log units. Similar differences of 2.79 log units (1.24 vs 4.03 log μM) and 2.67 log units (1.58 vs 4.25 log μM) were found, respectively, using a moderate zone III stimulus (Fig. 6C, D) and a weaker zone II stimulus (Fig. 6E, F). These findings suggested that applied 200 μM DHK has a stronger effect than the applied 0.5μM TBOA on increasing the potency of exogenous GLU, possibly through blocking the activities of membrane EAATs for removing free GLU.

By pooling the above data with the LAP4 data presented in section 3.2 of the companion paper, Fig. 7 compares the dose-response curves of GLU under 3 different conditions (injected alone, coinjected with DHK, or coinjected with TBOA) to the curve of LAP4. As illustrated, LAP4 has IC50 values 2.9–3.6 log units smaller than those of GLU. It is shown that GLU had its dose-response curves shifted largely towards the left when coinjected with DHK. The magnitudes of those left-shifts, when quantified using the IC50 values, was most prominent in zone IV and was equivalent to 86% of the difference in IC50 between GLU and LAP4. Equivalent shifts in IC50 were 72% and 74% in zone III and II, respectively. These suggest that EAAT2, selectively inhibited by the applied DHK, contributes to the removal of free synaptic glutamate in the photoreceptor-DBC synapses particularly in the cone-DBC synapses. These also indicate that the activity of EAAT2 was responsible for the difference between LAP4 and GLU in their potencies in inhibiting the b-wave.

In contrast, the presence of a threshold dose of TBOA did not consistently shift the GLU dose-response curve despite the fact that TBOA is a known non-specific EAAT blocker. In

our companion paper, we have shown that TBOA effectively inhibited the b-wave in a dose-dependent manner. 200μM DHK or 0.5μM TBOA inhibited the b-wave by a similar percentage when injected alone. If TBOA and DHK inhibited the b-wave through the same mechanism (blocking synaptic glutamate clearing), then co-injecting GLU with them at their respective threshold concentrations should have shifted the respective measured GLU dose-response curves. Our finding that such left-shifting occurred only in the presence of DHK but not TBOA indicates that TBOA inhibited the b-wave through a different mechanism when applied at the selected low concentration, without significantly affecting the clearing activity for free synaptic GLU. Such mechanism was studied in our companion paper and was found to be mediated by the blockage of postsynaptic EAAT5-coupled chloride channels on the DBCs. We did not study the effect of coinjecting GLU with a high concentration TBOA. It is expected that the clearing activity for free synaptic GLU will be affected if TBOA is applied in high concentrations.

3.4 Immunohistochemistry

To anatomically identify and localize the hardware underlying the observed DHK-sensitive glutamate removal mechanism, a series of IHC experiments were performed using a combination of antibodies that label different neurons in the OPL. Fig 8A shows that EAAT2a immuno-reactivity is present in multiple layers of the retina and is most prominent in the OPL. Fig. 8B shows that EAAT2a was not present on the presynaptic active zone of the cone pedicles. Fig. 8C shows that EAAT2a co-localized with PSD95 and suggested its presence on the rod terminal spherules. The absence of EAAT2a staining below the cone pedicles (Fig. 8D) indicated that DBC_C dendrites post-synaptic to cones did not express EAAT2a. In contrast, the finding that EAAT2a co-localized with PKCα suggested its presence on DBC_R dendrites (Fig. 8E–G).

EAAT2b immuno-reactivity was also most prominent in the OPL (Fig. 9A). Different from that of EAAT2a, EAAT2b was shown to be present on the active zone of cone pedicles (Fig. 9B,C). It was found in the distal half of the OPL staining numerous spherical shapes, resembling rod spherules, but not in the other half of the OPL proximal to the cone pedicles (Fig. 9B). EAAT2b appeared to be absent from DBC_Cs and DBC_Rs as no obvious colocalization with PKCα or Goα was observed (Fig. 9C,D).

4 DISCUSSION

The present paper is the first to study the in-vivo glutamate clearing activity of EAATs in intact living mouse retina, by taking advantage of an infrared illuminated microinjection system, the non-invasive ERG technique and the newly available EAAT1 specific blocker UCPH101.

4.1 EAAT2 contributes substantially to the GLU clearing activity in photoreceptor output synapses

We showed that the ERG b-wave was suppressed immediately after injection of exogenous GLU, and recovered gradually afterwards. The IC50 value for such GLU induced inhibition was found to be 3.58 log μM, which was 3.26 log units higher than that of LAP4 measured

with a zone III stimulus (Fig. 7B). Except for the above difference in potency, the patterns of GLU and LAP4 inhibition on the b-wave appeared qualitatively similar. This likely implies that GLU and LAP4 inhibited the b-wave through the same mechanism (saturating mGluR6) at the photoreceptor-DBC synapse, and that the lower potency of glutamate was possibly due to the selective affinity of EAATs for GLU but not LAP4. Because the ERG b-wave is generated by DBCs receiving synaptic input from the photoreceptors, the differences in their dose-response curves or IC50 values are likely indirect quantitative measures for the glutamate clearing activity at the photoreceptor synapse and along the diffusion pathway from the injected site to the synapse. The first line of evidence supporting this notion is provided by our IHC results, which confirmed the presence of EAAT2b on cone terminals, and the presence of EAAT2a, EAAT2b and EAAT5 (see companion paper for EAAT5 findings) on rod terminals.

Furthermore, coinjecting a low concentration (0.2mM) of DHK (a EAAT2 blocker) with GLU increased the potency of GLU drastically for inhibiting the b-wave. As illustrated in figure 7, the resultant GLU dose-response curve left-shifted to an extent more than half of the total difference between GLU and LAP4 for all three stimulus strengths when compared using the IC50 values. This second line of evidence strongly indicates that the glutamate clearing activity in both rod-DBC and cone-DBC synapses have been largely neutralized by DHK, and that the underlying EAAT subtype was the DHK-sensitive EAAT2. Moreover, the left-shifting of $IC50_{GLU}$ was most obvious in zone IV (Fig 7A) where the left-shifted $IC50_{GLU}$ became insignificantly different from the $IC50_{LAP4}$. This correlates well with our IHC results which showed that cone presynaptic active zones express only EAAT2, while rod presynaptic active zones express both EAAT2 and EAAT5. The absence of a second EAAT type on cone terminals may have rendered its GLU clearing capacity more susceptible for DHK.

4.2 Selective inhibition of EAAT1 but not EAAT2 disrupts GLU equilibrium in photoreceptor synapses and reduces the b-wave

Our data showed that temporarily blocking EAAT1 using injected UCPH partially inhibited the b-wave. Compared to other EAAT blockers, the effect of UCPH was slower.

It is possible that the slow time course of UCPH inhibition was a result of slower migration of UCPH molecule form the injection site to the Muller cells. Unlike the other tested drugs, UCPH is soluble in DMSO, poorly soluble in water, and has a heavier molecular weight (UCPH: 422, DHK: 215, TBOA: 239). Partial reductions in the b-wave amplitudes, similar to those produced by UCPH, have also been reported previously when EAAT1 was being suppressed permanently through genetic knockout (Harada, Harada et al. 1998) or by antisense oligonucleotide administration (Barnett and Pow 2000). Inhibition on the ERG b-wave produced by injecting antisense oligonucleotide was also slow. In mouse retina, EAAT1 is not present on photoreceptor terminals but on Müller cells, which wrap around the photoreceptor-DBC synapse. It may function as a GLU reuptake mechanism in the synapse, and its inhibition may have led to the accumulation of endogenous GLU in the synapse, or a perturbed glutamate-glutamine recycling between Müller cells and photoreceptors (Pow and Robinson 1994), and subsequently an inhibition of the b-wave. An

alternative explanation for the slow action of UCPH is that accumulation of synaptic GLU was slow, when the other EAATs at the synapse remained functional.

In contrast, blocking EAAT2 alone did not significantly inhibit the b-wave. Our data showed that 0.2mM DHK effectively shifted the GLU dose-response curve when coinjected, but has little effect on the b-wave when injected alone. This suggests that blocking EAAT2 alone does not cause accumulation of endogenous GLU in the photoreceptor-DBC synapse in the presence of functional EAAT1. The fact that selectively blocking EAAT1 produced stronger inhibition on the b-wave than selectively blocking EAAT2 is intriguing, because EAAT2 has a similar affinity for GLU (Arriza, Fairman et al. 1994), a faster turnover rate (Bergles and Jahr 1998; Wadiche and Kavanaugh 1998) compared to EAAT1, and is located closer to the GLU release site. One possible explanation is that the total number of EAAT1 transporters may be much higher than that of EAAT2 at the synapse, so that its blockage resulted in a higher impact on the overall GLU removing capacity and the accumulation of GLU.

A higher concentration of DHK (15mM) inhibited the ERG b-wave though when injected alone. At higher stimulus levels within the operational range of cones, inhibition was weaker at the beginning but developed gradually with time during the one hour period tested (Fig. 3A). A different time course was observed at lower stimulus levels at which only rods were functional. Since we have shown in the co-injection experiment that 0.2mM DHK was very effective in inhibiting the GLU clearing activity of EAAT2, this direct inhibition of the b-wave by a higher concentration DHK probably involved a second mechanism. Given that DHK is 130-fold more selective for EAAT2 (K_i = 23 μM) over EAAT1 ($K_i \geq 3$ mM), we postulate that DHK non-specific blocking of EAAT1 was responsible. In our ERG results, the time course for inhibition of the b-wave was much faster in the rod operative range. This may imply that rod-DBC synapses, compared to cone-DBC synapses, are more dependent on the EAAT1 on Müller cells to maintain its GLU equilibrium. Alternatively, it is also possible that the fast onset inhibition of the b-wave following injection resulted from a direct inhibition of post-synaptic EAAT2a on DBC_R by DHK. This blocked the EAAT gated chloride channel in the dark, making the membrane resting potential less hyperpolarized and subsequently reduced the b-wave generated by the DBC_R during the light-elicited depolarization. It has been reported that EAAT2 mediates a small but measurable chloride conductance (Wadiche, Amara et al. 1995), compared to that of EAAT5 (Arriza, Eliasof et al. 1997).

4.3 EAAT5 inhibited the b-wave without significantly affecting the glutamate clearing capacity

Our data has shown that the presence of co-injected TBOA did not consistently shift the GLU dose-response curves. TBOA is a known inhibitor for EAAT 1–5, and should have left-shifted the GLU dose-response curve if it had functioned like DHK and blocked the presynaptic EAATs in the synapse. The best explanation for this result is that the applied TBOA concentration (0.5μM) was too low to effectively neutralize the GLU clearing capacity of EAATs in the photoreceptor-DBC synapse. Given the fact that the same concentration of TBOA inhibited the b-wave by 16–23% and 45–48% in wildtype and

bhlhb4 −/− mice, respectively, when injected alone (see section 3.3 of the companion paper), it is indicated that the mechanism through which low concentration TBOA inhibited the b-wave did not involve blockage of presynaptic EAATs and saturation of synaptic GLU. EAAT5 is known for its dual functions of GLU transporter and GLU-gated chloride channels (Sonders and Amara 1996; Arriza, Eliasof et al. 1997). We presented evidences in our companion paper that the above inhibition was mediated through the EAAT5-coupled chloride channel on cone depolarizing bipolar cell dendrites.

4.4 Rod-DBCc synapse is more susceptible to inhibition by exogenous GLU

Our results have shown that the b-wave measured with zone III stimuli was inhibited most strongly by exogenous GLU (Fig. 1B, C). It has been previously characterized that the Rod-DBCc pathway is particularly active at that intensity (Abd-El-Barr, Pennesi et al. 2009). This indicates that the Rod-DBC_C synapse is more susceptible to influence by exogenous GLU. One possible explanation for this could be that the Rod-DBC_C synapse has a weaker diffusion barrier for exogenous molecules compared to other photoreceptor-to-DBC synapses.

4.5 Conclusion

The present study has provided electrophysiological, pharmacological and immunohistological evidences for the functions of EAAT1 on Müller cells, EAAT2b on cone terminals, and the functions of EAAT2a, EAAT2b and EAAT5 on rod terminals in intact dark-adapted retinae of living mice. Selective inhibition of EAAT1 using a newly available blocker (UCPH101) has led to reductions in the b-wave suggesting that the EAAT1 on Müller cells is necessary to maintain proper photoreceptor-to-DBC signal transmission by acting as the major GLU reuptake mechanism, which is characterized by a slower turnover rate but an overall higher clearing capacity. The b-wave was inhibited by selective inhibition of EAAT1, but not selective inhibition of EAAT2, suggesting that EAAT1 plays a dominating role in GLU reuptake in the synaptic cleft. The clearing activity for exogenous GLU at the cone and rod terminals can be neutralized largely by DHK, indicating that it is mediated by EAAT2 at the photoreceptor-DBC synapse. The close proximity of EAAT2 to the GLU release site and its higher turnover rate imply a significant role of EAAT2 in the timely reabsorption of GLU to the photoreceptor terminal. Low concentration of non-specific EAAT blocker (TBOA) inhibited the b-wave without affecting the GLU clearing activity, suggesting the presence of a TBOA-sensitive postsynaptic receptor in the synapse.

ACKNOWLEDGMENTS

We thank J.J. Pang for suggestions and comments, Z. Yang for technical support, R Jacoby for carefully reading manuscript and helpful comments.

GRANTS

This work was supported by NIH EY004446 & EY019908, NIH Vision Core EY02520, the Retina Research Foundation(Houston), Research to Prevent Blindness Inc, and the International Retinal Research Foundation Loris and David Rich Postdoctoral Scholar Award.

Abbreviations

ERG	electroretinogram
BC	bipolar cell
EAAT	excitatory amino-acid transporter
GLT	Glial Glutamate Transporter
GLU	L-glutamic acid
LAP4	L-(+)-2-amino-4-phosphonobutyric acid
DHK	Dihydrokainic acid
TBOA	DL-threo-β-benzyloxyaspartic acid
UCPH	2-Amino-5,6,7,8-tetrahydro-4-(4-met-hoxyphenyl)-7-(naphthalen-1 -yl)-5-oxo-4H-chromene--3-carbonitrile
ONL	outer nuclear layer
OPL	outer plexiform layer
INL	inner nuclear layer
IPL	inner plexiform layer
IC50	half maximal inhibitory concentration
EC50	half maximal effective concentration
DBC_R	rod depolarizing bipolar cell
DBC	epolarizing bipolar cell
IHC	mmunohistochemistry

REFERENCES

Abd-El-Barr MM, Pennesi ME, et al. Genetic dissection of rod and cone pathways in the dark-adapted mouse retina. Journal of neurophysiology. 2009; 102(3):1945–1955. [PubMed: 19587322]

Applebury ML, Antoch MP, et al. The murine cone photoreceptor: a single cone type expresses both S and M opsins with retinal spatial patterning. Neuron. 2000; 27(3):513–523. [PubMed: 11055434]

Arriza JL, Eliasof S, et al. Excitatory amino acid transporter 5, a retinal glutamate transporter coupled to a chloride conductance. Proceedings of the National Academy of Sciences of the United States of America. 1997; 94(8):4155–4160. [PubMed: 9108121]

Arriza JL, Fairman WA, et al. Functional comparisons of three glutamate transporter subtypes cloned from human motor cortex. The Journal of neuroscience : the official journal of the Society for Neuroscience. 1994; 14(9):5559–5569. [PubMed: 7521911]

Attwell, D. The photoreceptor output synapse. Progress in Retinal Research. Osborne, N.; Chader, G., editors. Oxford: Pergamon Press; 1990. p. 9

Barnett NL, Pow DV. Antisense knockdown of GLAST, a glial glutamate transporter, compromises retinal function. Investigative ophthalmology & visual science. 2000; 41(2):585–591. [PubMed: 10670492]

Baylor DA, Fuortes MG. Electrical responses of single cones in the retina of the turtle. The Journal of physiology. 1970; 207(1):77–92. [PubMed: 4100807]

Bergles DE, Jahr CE. Glial contribution to glutamate uptake at Schaffer collateral- commissural synapses in the hippocampus. The Journal of neuroscience : the official journal of the Society for Neuroscience. 1998; 18(19):7709–7716. [PubMed: 9742141]

Blanks JC, Johnson LV. Selective lectin binding of the developing mouse retina. The Journal of comparative neurology. 1983; 221(1):31–41. [PubMed: 6643744]

Cervetto L, MacNichol EF Jr. Inactivation of horizontal cells in turtle retina by glutamate and aspartate. Science. 1972; 178(4062):767–768. [PubMed: 5082843]

Copenhagen DR, Jahr CE. Release of endogenous excitatory amino acids from turtle photoreceptors. Nature. 1989; 341(6242):536–539. [PubMed: 2477707]

Danbolt NC. Glutamate uptake. Progress in neurobiology. 2001; 65(1):1–105. [PubMed: 11369436]

de Melo J, Qiu X, et al. Dlx1, Dlx2, Pax6, Brn3b, and Chx10 homeobox gene expression defines the retinal ganglion and inner nuclear layers of the developing and adult mouse retina. The Journal of comparative neurology. 2003; 461(2):187–204. [PubMed: 12724837]

Diamond JS, Jahr CE. Transporters buffer synaptically released glutamate on a submillisecond time scale. The Journal of neuroscience : the official journal of the Society for Neuroscience. 1997; 17(12):4672–4687. [PubMed: 9169528]

Dowling JE, Ripps H. Effect of magnesium on horizontal cell activity in the skate retina. Nature. 1973; 242(5393):101–103. [PubMed: 4348460]

Field GD, Rieke F. Nonlinear signal transfer from mouse rods to bipolar cells and implications for visual sensitivity. Neuron. 2002; 34(5):773–785. [PubMed: 12062023]

Gao H, Pennesi ME, et al. Intravitreal moxifloxacin: retinal safety study with electroretinography and histopathology in animal models. Invest Ophthalmol Vis Sci. 2006; 47(4):1606–1611. [PubMed: 16565399]

Granit R. The components of the retinal action potential in mammals and their relation to the discharge in the optic nerve. The Journal of physiology. 1933; 77(3):207–239. [PubMed: 16994385]

Harada T, Harada C, et al. Functions of the two glutamate transporters GLAST and GLT-1 in the retina. Proceedings of the National Academy of Sciences of the United States of America. 1998; 95(8):4663–4666. [PubMed: 9539795]

Hasegawa J, Obara T, et al. High-density presynaptic transporters are required for glutamate removal from the first visual synapse. Neuron. 2006; 50(1):63–74. [PubMed: 16600856]

Haverkamp S, Wassle H. Immunocytochemical analysis of the mouse retina. The Journal of comparative neurology. 2000; 424(1):1–23. [PubMed: 10888735]

Hertz L, Dringen R, et al. Astrocytes: glutamate producers for neurons. Journal of neuroscience research. 1999; 57(4):417–428. [PubMed: 10440891]

Lyubarsky AL, Daniele LL, et al. From candelas to photoisomerizations in the mouse eye by rhodopsin bleaching in situ and the light-rearing dependence of the major components of the mouse ERG. Vision research. 2004; 44(28):3235–3251. [PubMed: 15535992]

Massey, SC. Cell types using glutamate as a neurotransmitter in the vertebrate retina. Progress in Retinal Research. Osborne, N.; Chader, G., editors. Oxford: Pergamon Press; 1990. p. 9

Massey SC, Redburn DA. Transmitter circuits in the vertebrate retina. Progress in neurobiology. 1987; 28(1):55–96. [PubMed: 2881324]

Murakami M, Otsuka T, et al. Effects of aspartate and glutamate on the bipolar cells in the carp retina. Vision research. 1975; 15(3):456–458. [PubMed: 166508]

Nikonov SS, Kholodenko R, et al. Physiological features of the S- and M-cone photoreceptors of wild-type mice from single-cell recordings. The Journal of general physiology. 2006; 127(4):359–374. [PubMed: 16567464]

Oh EC, Khan N, et al. Transformation of cone precursors to functional rod photoreceptors by bZIP transcription factor NRL. Proceedings of the National Academy of Sciences of the United States of America. 2007; 104(5):1679–1684. [PubMed: 17242361]

Pang JJ, Gao F, et al. Light-evoked current responses in rod bipolar cells, cone depolarizing bipolar cells and AII amacrine cells in dark-adapted mouse retina. The Journal of physiology. 2004; 558(Pt 3):897–912. [PubMed: 15181169]

Pow DV, Robinson SR. Glutamate in some retinal neurons is derived solely from glia. Neuroscience. 1994; 60(2):355–366. [PubMed: 7915410]

Rauen T, Kanner BI. Localization of the glutamate transporter GLT-1 in rat and macaque monkey retinae. Neuroscience letters. 1994; 169(1–2):137–140. [PubMed: 8047270]

Rauen T, Rothstein JD, et al. Differential expression of three glutamate transporter subtypes in the rat retina. Cell and tissue research. 1996; 286(3):325–336. [PubMed: 8929335]

Reye P, Sullivan R, et al. Distribution of two splice variants of the glutamate transporter GLT1 in the retinas of humans, monkeys, rabbits, rats, cats, and chickens. The Journal of comparative neurology. 2002; 445(1):1–12. [PubMed: 11891650]

Rose EM, Koo JC, et al. Glutamate transporter coupling to Na,K-ATPase. The Journal of neuroscience : the official journal of the Society for Neuroscience. 2009; 29(25):8143–8155. [PubMed: 19553454]

Rothstein JD, Dykes-Hoberg M, et al. Knockout of glutamate transporters reveals a major role for astroglial transport in excitotoxicity and clearance of glutamate. Neuron. 1996; 16(3):675–686. [PubMed: 8785064]

Saszik SM, Robson JG, et al. The scotopic threshold response of the dark-adapted electroretinogram of the mouse. The Journal of physiology. 2002; 543(Pt 3):899–916. [PubMed: 12231647]

Schultz K, Stell WK. Immunocytochemical localization of the high-affinity glutamate transporter, EAAC1, in the retina of representative vertebrate species. Neuroscience letters. 1996; 211(3):191–194. [PubMed: 8817573]

Shigeri Y, Seal RP, et al. Molecular pharmacology of glutamate transporters, EAATs and VGLUTs. Brain research. Brain research reviews. 2004; 45(3):250–265. [PubMed: 15210307]

Sonders MS, Amara SG. Channels in transporters. Current opinion in neurobiology. 1996; 6(3):294–302. [PubMed: 8794089]

Tanaka K, Watase K, et al. Epilepsy and exacerbation of brain injury in mice lacking the glutamate transporter GLT-1. Science. 1997; 276(5319):1699–1702. [PubMed: 9180080]

Tong G, Jahr CE. Block of glutamate transporters potentiates postsynaptic excitation. Neuron. 1994; 13(5):1195–1203. [PubMed: 7946356]

Wadiche JI, Amara SG, et al. Ion fluxes associated with excitatory amino acid transport. Neuron. 1995; 15(3):721–728. [PubMed: 7546750]

Wadiche JI, Arriza JL, et al. Kinetics of a human glutamate transporter. Neuron. 1995; 14(5):1019–1027. [PubMed: 7748550]

Wadiche JI, Kavanaugh MP. Macroscopic and microscopic properties of a cloned glutamate transporter/chloride channel. The Journal of neuroscience : the official journal of the Society for Neuroscience. 1998; 18(19):7650–7661. [PubMed: 9742136]

Ward MM, Jobling AI, et al. Localization and expression of the glutamate transporter, excitatory amino acid transporter 4, within astrocytes of the rat retina. Cell and tissue research. 2004; 315(3): 305–310. [PubMed: 14727177]

Watase K, Hashimoto K, et al. Motor discoordination and increased susceptibility to cerebellar injury in GLAST mutant mice. The European journal of neuroscience. 1998; 10(3):976–988. [PubMed: 9753165]

Wersinger E, Schwab Y, et al. The glutamate transporter EAAT5 works as a presynaptic receptor in mouse rod bipolar cells. The Journal of physiology. 2006; 577(Pt 1):221–234. [PubMed: 16973698]

Winkler BS, Kapousta-Bruneau N, et al. Effects of inhibiting glutamine synthetase and blocking glutamate uptake on b-wave generation in the isolated rat retina. Visual neuroscience. 1999; 16(2): 345–353. [PubMed: 10367968]

Zhang J, Yang Z, et al. Development of cholinergic amacrine cells is visual activity-dependent in the postnatal mouse retina. The Journal of comparative neurology. 2005; 484(3):331–343. [PubMed: 15739235]

Highlights

- Intravitreally injected glutamate inhibited the mouse ERG b-wave with a low potency
- EAAT1 and EAAT2 contribute primarily to the clearance of synaptic glutamate.
- Blocking EAAT1 inhibited the b-wave likely via accumulation of endogenous glutamate.
- Blocking EAAT2 increased the potency of injected glutamate in inhibiting the b-wave.
- The spatial distribution of EAAT2 splice variants was studied using immunohistochemistry

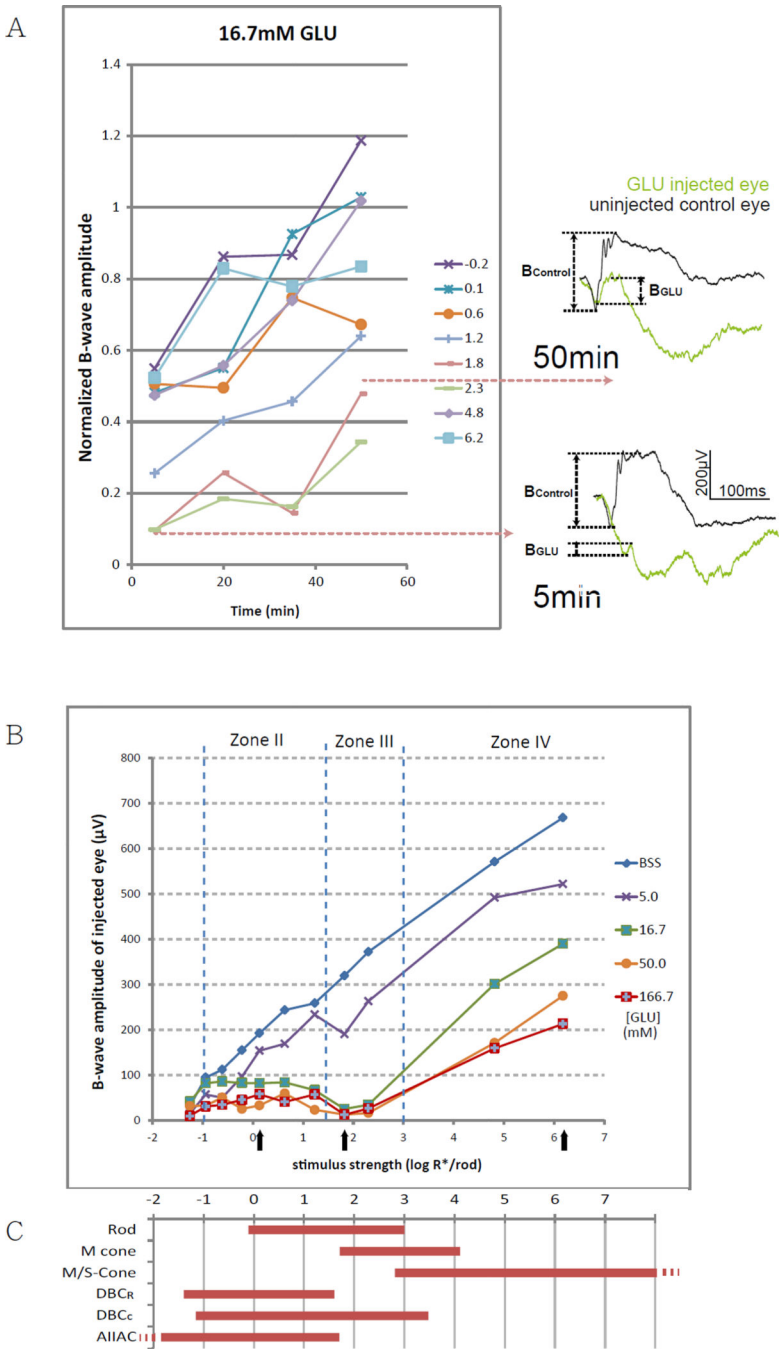

Figure 1.

(A) Changes of b-wave amplitude over time after applying 16.7mM (retinal concentration) GLU. Lines represent corresponding strengths of stimulus in log R*/Rod. ERGs on the right are representative raw traces measured using a stimulus of 1.8 log R*/Rod at the 5 min and the 50 min time points. Normalized b-wave amplitudes were the lowest at 5 min and increased with time, implying that GLU inhibits the b-wave through a fast acting mechanism.

(B) A line chart showing b-wave amplitude against stimulus strength in eyes 5 min after being injected with different concentrations of GLU. The vertical dotted lines define the stimulus range into zones II, III and IV, according to the dynamic ranges of various retinal neurons. Inhibition of the b-wave was the strongest at zone III, where the direct rod-DBCc pathway is operational. Black arrows denote the three representative strengths for fitting the dose-response curves in the other figures.

(C) Dynamic ranges (defined as 5–95% of maximum response) of various retinal neurons measured in wild type mice. Rod, M- and S-cone data are from suction-electrode recording from outer segments (Field and Rieke 2002; Nikonov, Kholodenko et al. 2006). M/S-cone range is extrapolated from the fact that many cones co-express both pigments (Applebury, Antoch et al. 2000). Ranges for DBC_R, DBC_C, and AIIAC are from light-evoked voltage-clamp results (Pang, Gao et al. 2004).

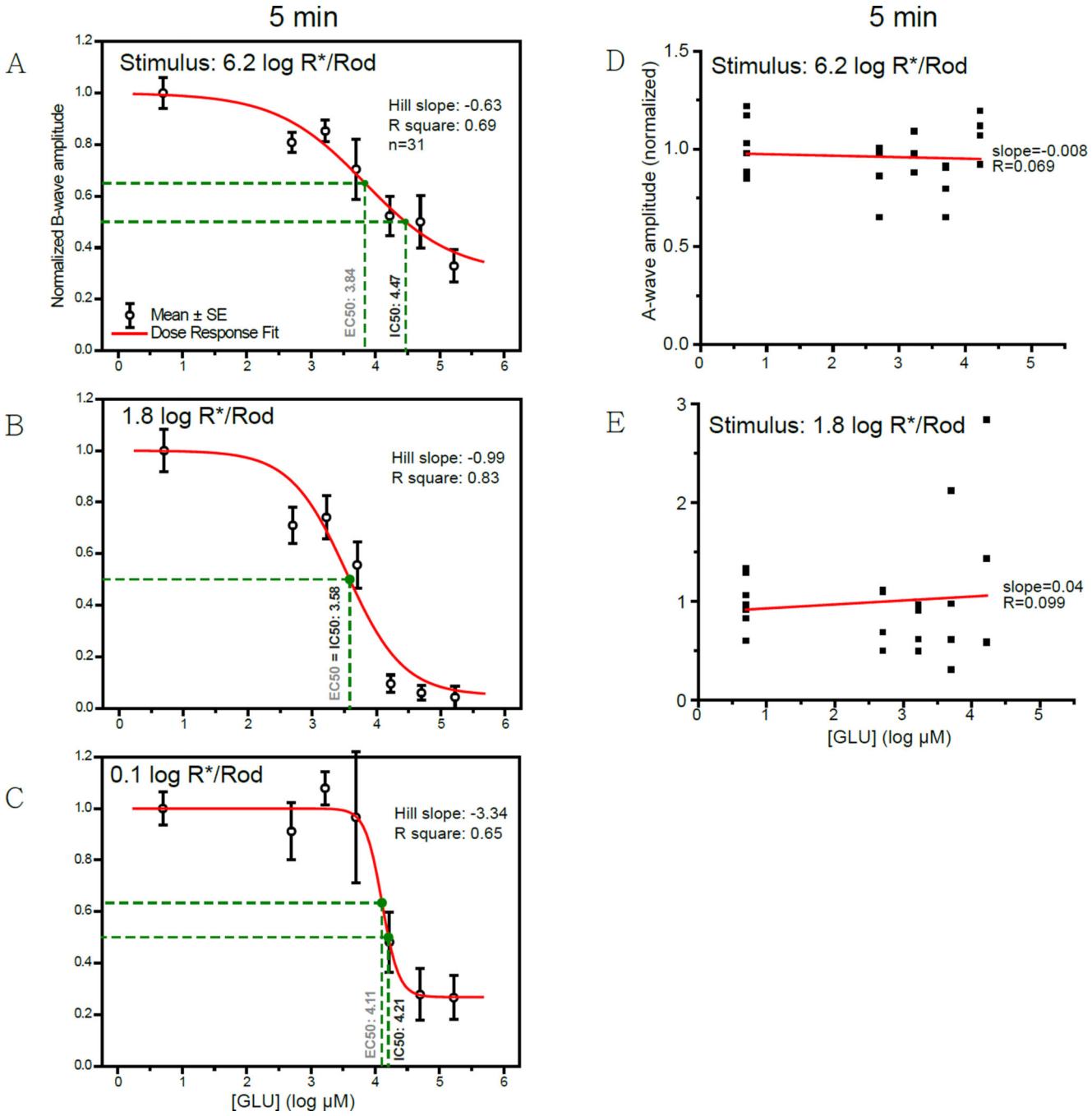

Figure 2.

(A–C) Dose-response curves showing the amplitude of b-wave against log concentration of GLU measured at three different stimulus levels. Individual data points and error bars denote value mean and standard error, respectively. Values in black and gray beside the vertical drop-lines represent IC50 and EC50, respectively. (A) Curve measured with a strong rod-saturating zone IV stimulus within the operating range of cones. B-wave was inhibited by 67% with highest concentrations of GLU. (B) Curve measured with a moderate zone III stimulus. The b-wave was almost completely inhibited (96%) when concentrations were

high enough. (C) Curve measured with a weaker zone II stimulus. The b-wave was greatly inhibited by the highest concentrations of GLU, with a residual of about 27%. (D,E) Scatterplots showing the normalized amplitude of a-wave versus the concentration of GLU measured with (D) a strong stimulus of 6.2 log R*/Rod or (E) a moderate stimulus of 1.8 log R*/Rod. The A-wave amplitude became more variable when GLU concentrations were high. The slopes for the linear regression lines were −0.008 and 0.099, quite close to zero, indicating that the amplitude of a-wave did not correlate with the concentration of GLU.

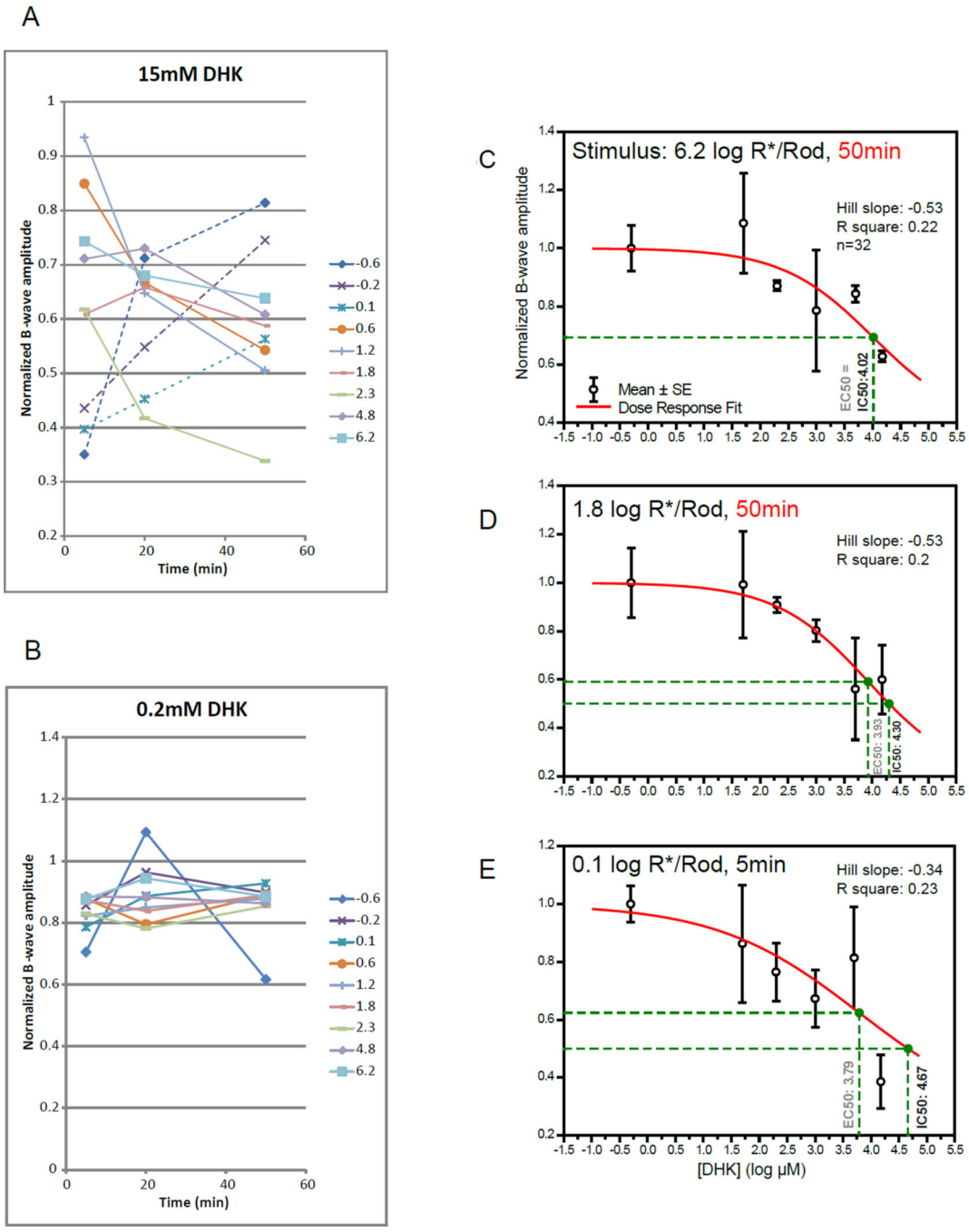

Figure 3.

(A) A line chart showing the changes in normalized b-wave amplitude 5 to 50 min after injecting DHK of 15mM (retinal concentration). Lines represent corresponding stimulus strengths in log photoisomerizations per rod (R*/rod). Two different trends were observed. First, b-wave amplitudes decreased with time and were the lowest at the 50 min point for stimuli (solid lines) of 0.6 log R*/rod or stronger. This implies that DHK inhibited the b-wave through a slow acting mechanism in this stimulus range. Second, b-wave amplitudes were the lowest at the 5 min point and increased with time for stimulus strengths (dotted

lines) between −0.6 to 0.1 log R*/rod. This implies that DHK inhibited the b-wave through a fast acting mechanism in that range. (B) Injected 0.2mM DHK has a small inhibitory effect on the normalized b-wave.

(C–E) Dose-response curves showing normalized amplitude of b-wave against log concentrations of DHK measured at three different stimulus levels. Individual data points and error bars denote value mean and standard error, respectively. Values in black and gray beside the vertical drop-lines represent IC50 and EC50, respectively. Note that presented concentrations were calculated by diluting the injected aliquot with the vitreous volume, without accounting for possible clearance overtime. (C) Curve measured with a strong rod-saturating zone IV stimulus within the operating range of cones 50 min after injection. Mean b-wave was inhibited by 39% with the highest concentration. (D) A curve fitted using data measured with a moderate zone III stimulus 50 min after injection. Mean b-wave was inhibited by 40–44% with the two highest concentrations. (E) A curve fitted using data measured with a weaker zone II stimulus 5 min post-injection. Mean b-wave was inhibited by 62% with the highest concentration.

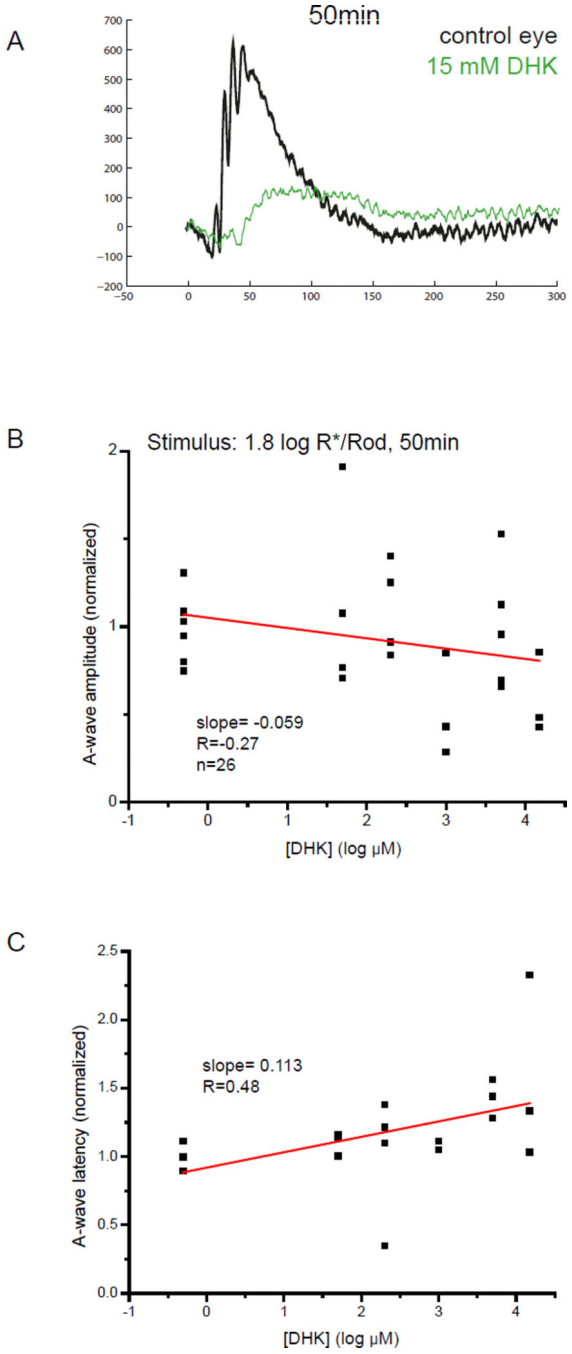

Figure 4.

(A) Representative raw wave traces showing a- and b-wave from an uninjected eye (black) and an eye injected with 15 mM retinal concentration of DHK. A consistent, large reduction in the amplitude of the b-wave was observed together with a minor reduction in the amplitude of the a-wave and significant increased latency of a-wave. (B) Scatterplot showing the normalized amplitude of a-wave versus log concentration of DHK measured with a zone III stimulus of 1.8 log R*/Rod. The slope for the linear regression line was −0.059, indicating that the amplitude of a-wave did not change with the concentration of

those agonists. (C) Scatterplot showing the normalized latency of a-wave versus log concentration of DHK measured with a zone III stimulus. The slope for the linear regression lines were 0.113, indicating that the latency of the a-wave barely increases with the concentration of DHK.

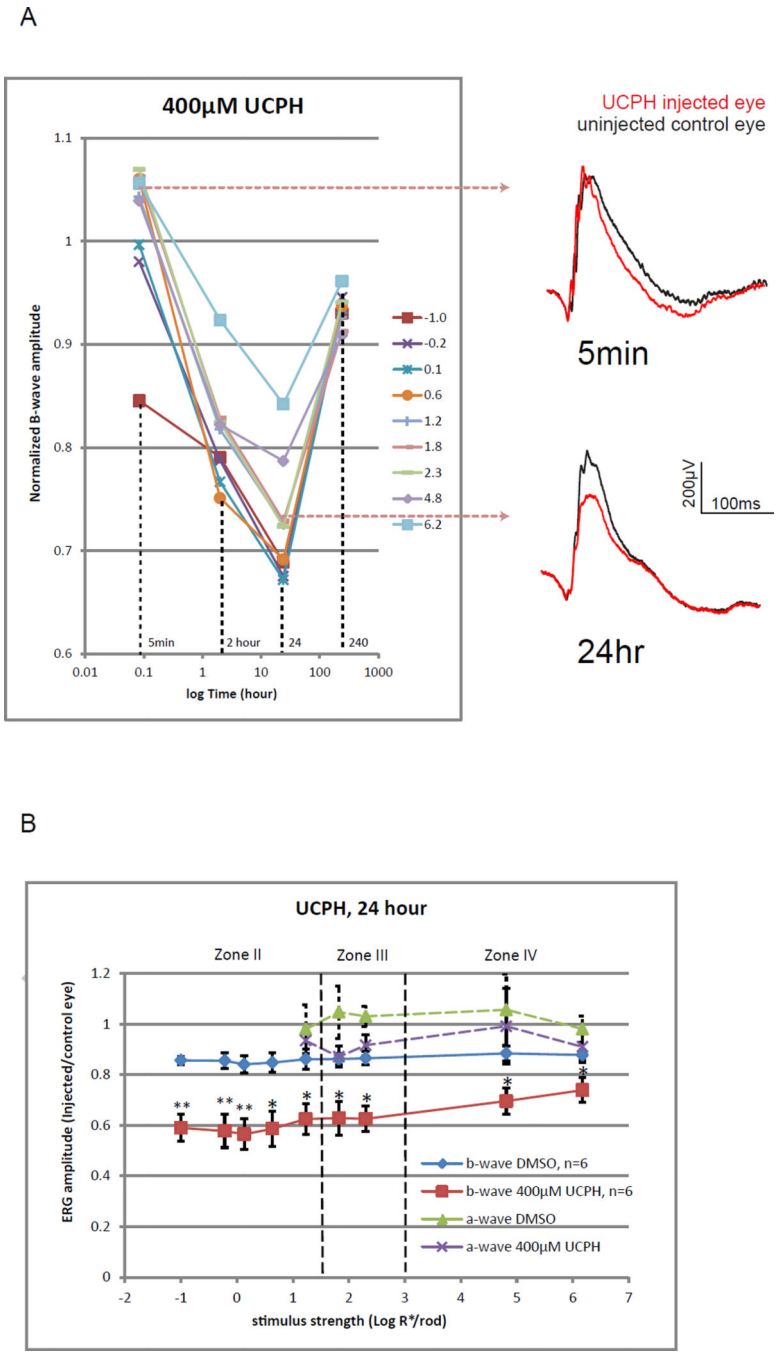

Figure 5.

(A) Changes of normalized b-wave amplitude over time after applying 400µM (retinal concentration) UCPH-101. Lines represent corresponding strengths of stimulus in log R*/Rod. Normalized b-wave amplitudes decreased with time and were the lowest at the 24th hour. The b-wave recovered mostly by the 10th day. ERGs on the right are representative raw traces measured using a stimulus of 1.8 log R*/Rod at the 5 min and the 24 hour time points.

(B) A line chart showing fractional b- and a-wave amplitude for a range of increasing stimulus strength for mice injected with DMSO alone or 400μM UCPH. Data points and error bars represent mean and standard error. Dashed lines represent boundaries between the II, III and IV zones of stimulus strength. Mean values that are significantly different from that of the DMSO group were marked with asterisks ($p<0.05$) or double asterisks ($p<0.01$). Compared to DMSO controls, UCPH significantly inhibited the b- wave in zones II, III and IV, with the strongest inhibition in zone II. In contrast, it did not significantly inhibit amplitudes of the a-wave.

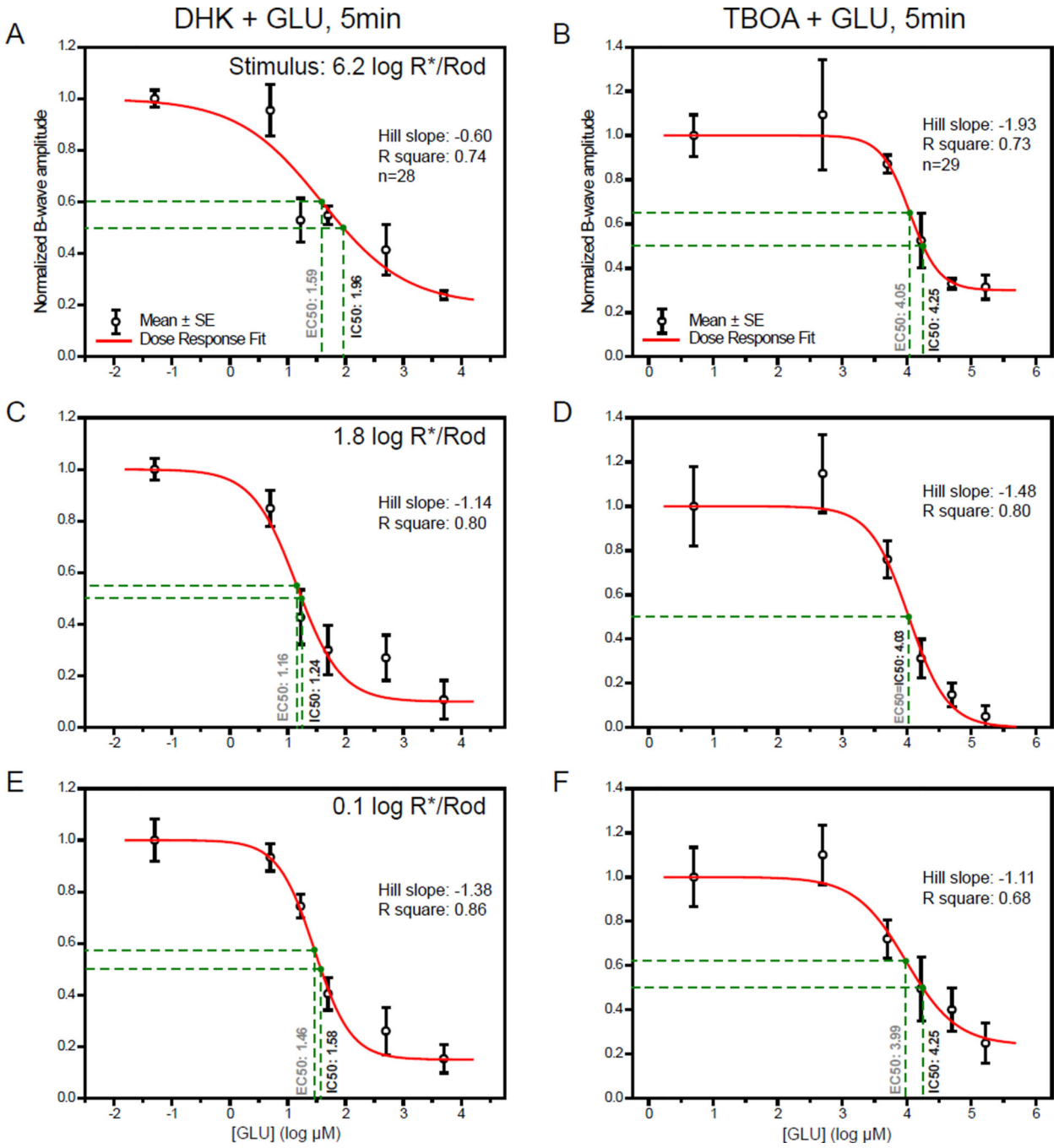

Figure 6.

Dose-response curves showing amplitudes of b-wave against log concentration of GLU measured at three different stimulus levels in the presence of either EAAT inhibitor. Individual data points and error bars denote value mean and standard error, respectively. Data were normalized to controls in which a threshold dose of the selected EAAT inhibitor, DHK or TBOA, was solely injected. Values in black and gray beside the vertical drop-lines represents IC50 and EC50, respectively.

(A,B) Dose-response curves measured with a strong rod-saturating zone IV stimulus within the operating range of cones. Using the highest concentration of GLU, the b-wave was inhibited by maximums of 76% and 69% when co-injected with DHK and TBOA, respectively.
(C,D) Curves measured with a moderate zone III stimulus. The b-wave was inhibited by maximums of 89% and 95%, nearly abolished, when co-injected with DHK and TBOA, respectively.
(E,F) Curves measured with a weaker zone II stimulus. The b-wave was largely reduced by about 85% and 75% when co-injected with DHK and TBOA, respectively. At all three stimulus strengths, GLU had lower EC50 and IC50 values when co-injected with DHK, compared to those co-injected with TBOA.

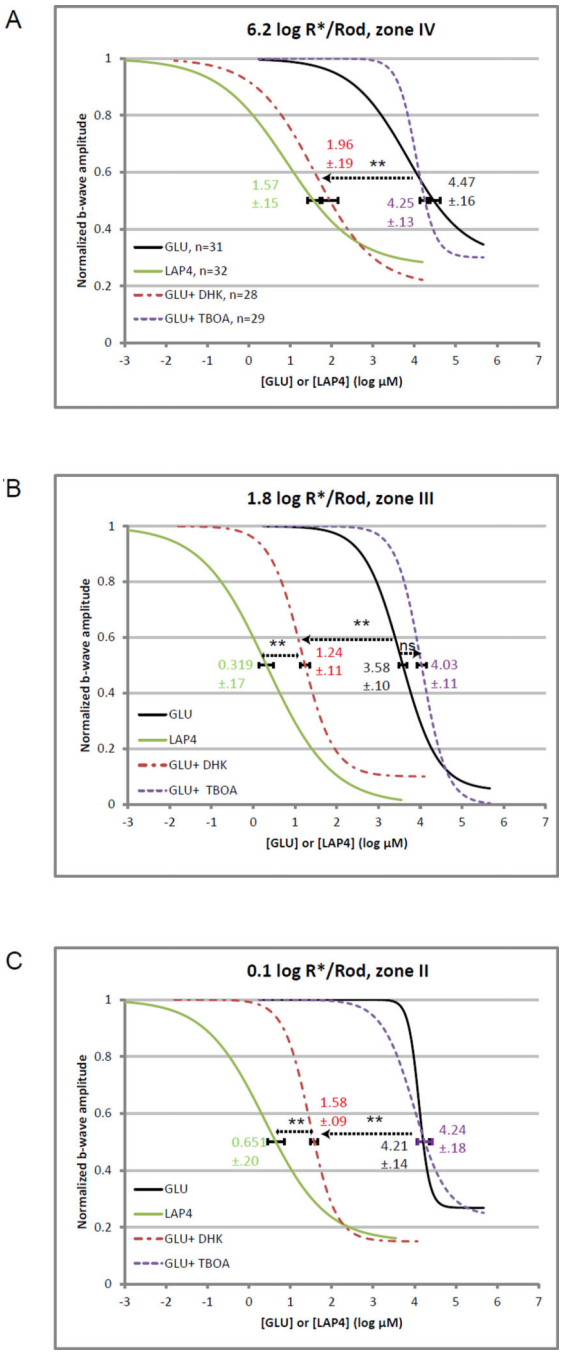

Figure 7.

Integrated line charts showing dose-response curves for LAP4, and for GLU under different conditions, at three levels of stimulus strength. Individual data points were not displayed to keep the figures clear. The numbers and error bars on individual curves denote the IC50 values and standard errors, respectively.

(A) Dose-response curves measured with a strong rod-saturating zone IV stimulus. LAP4 has an IC50 value 2.9 log units lower than that of GLU. The presence of DHK shifts the GLU curve to the left and significantly ($p<0.01$) reduces the IC50 value from 4.47 to 1.96

log μM (86% of the total difference between $IC50_{GLU}$ and $IC50_{LAP4}$). There was no difference between $IC50_{LAP4}$ and $IC50_{GLU+DHK}$ ($p>0.05$). Coinjecting with TBOA did not significantly shift the IC50 value for GLU ($p>0.05$).

(B) Dose-response curves measured with a moderate zone III stimulus. LAP4 has an IC50 value 3.2 log units lower than that of GLU. The presence of DHK shifts the GLU curve to the left and significantly ($p<0.01$) reduces its IC50 from 3.58 to 1.24 log μM (72% of the difference). TBOA has no significant effect on $IC50_{GLU}$.

(C) Dose-response curves measured with a scotopic zone II stimulus. LAP4 has an IC50 value 3.6 log units lower than that of GLU. The presence of DHK shifts the GLU curve to the left and significantly ($p<0.01$) reduces its IC50 from 4.21 to1.58 log μM (74% of the difference), while TBOA has little effect on $IC50_{GLU}$.

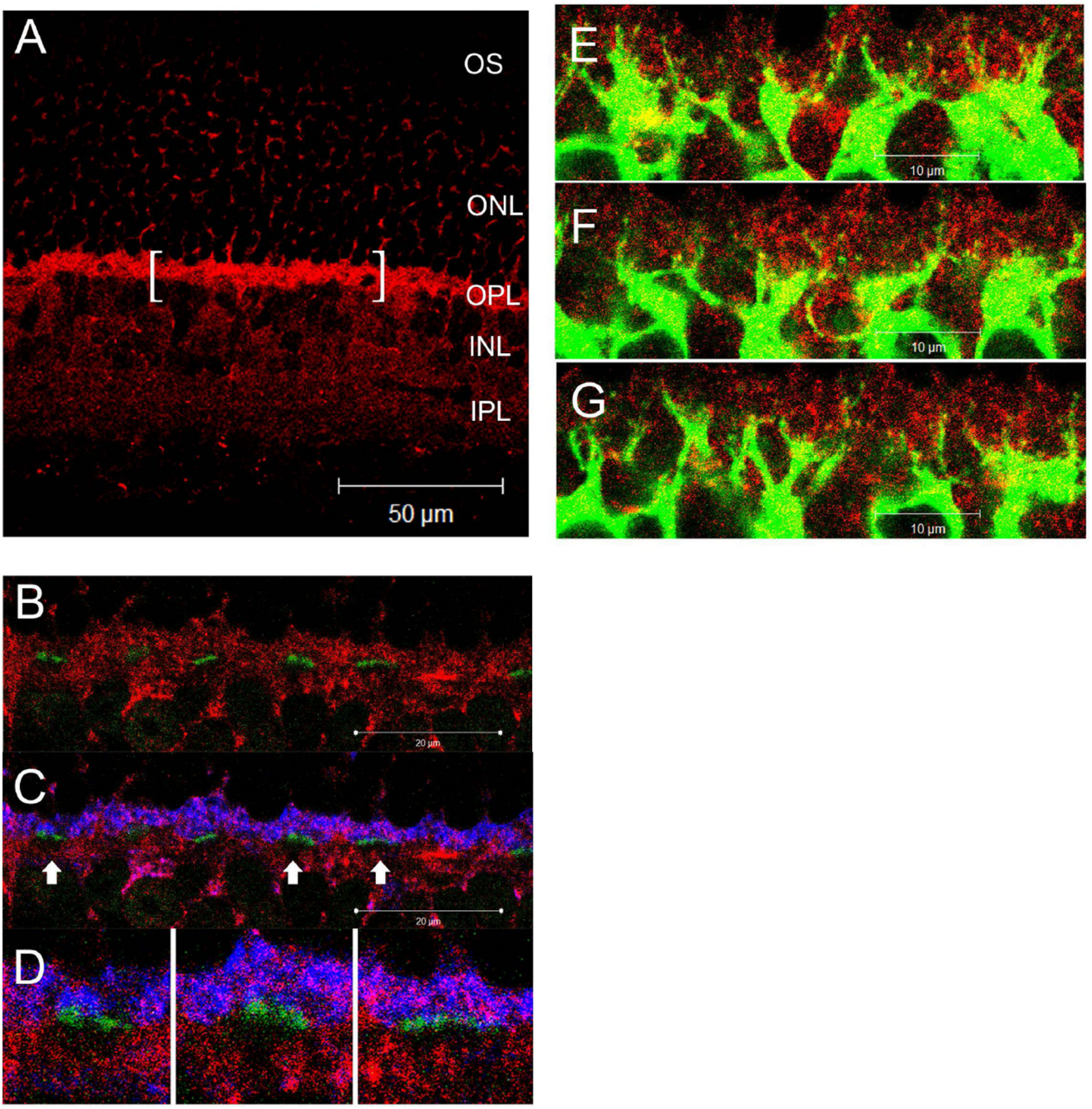

Figure 8.

(A–D) Confocal micrographs of retina from wild-type mice processed for EAAT2a (red), PSD95 (blue) and PNA (green). (A) EAAT2a immuno-reactivity (IR) was most prominent in the OPL, diffusely present in the IPL and sparsely present in the INL and ONL. The bracketed segment is presented in the next few panels at a higher magnification. (B) EAAT2a IR did not overlap with the PNA staining, indicating that EAAT2a is not present on the presynaptic active zones of cone photoreceptors. (C) PSD95-IR was present in the distal half of the OPL where it co-localized with EAAT2a staining. Regions denoted by

arrows were further magnified and presented in (D). (D) The EAAT2a–negative cavities under the PNA staining suggest that EAAT2a is not present on the dendritic processes of DBC_Cs that are post-synaptic to cones. (E–G) A z-axis image series of consecutive optical sections (1μm apart) showing the colocalization of EAAT2a (red) and PKCα (green) on DBC_R dendrites as yellow punctate staining.

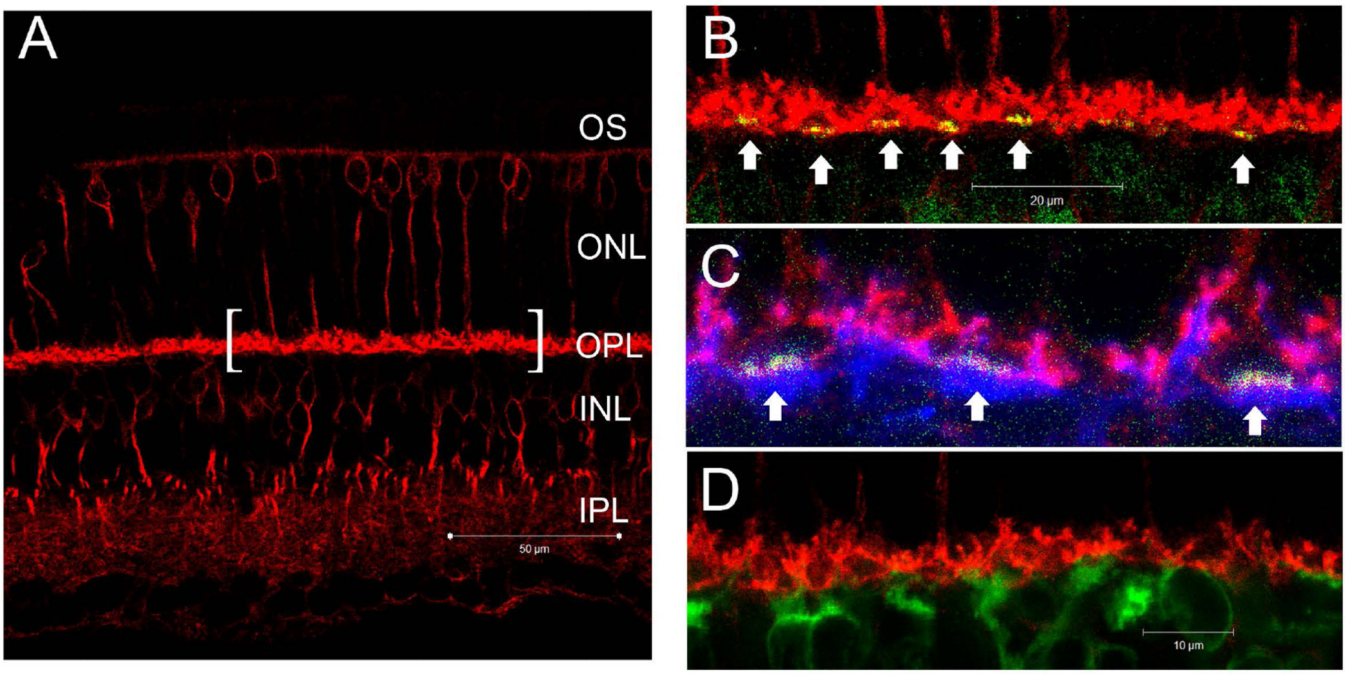

Figure 9.

(A–C) Confocal microscopic images of retina from wild-type mice processed for EAAT2b (red), Goα (blue) and PNA (green). (A) EAAT2b–IR presented prominently in the OPL, and diffusely in the IPL without clear stratification. Some of the somas (possible cones) in the ONL and INL were also stained. A segment of OPL is presented as (B) and (C) at higher magnification. (B) EAAT2b–IR was present only in the half of the OPL that is distal to PNA staining. The dense spherically shaped staining in red is likely rod terminals. On the other hand, overlapped staining of PNA and EAAT2b resulted in the yellow color on cone pedicles (arrows). (C) Goα-IR presented mainly in the half of the OPL that is proximal to PNA staining. There was no obvious overlapping between Goα and EAAT2b staining, suggesting that EAAT2b is not present on the dendrites of DBCs. (D) The lack of overlap between EAAT2b (red) and PKCα (green) staining suggests that EAAT2b is not present on DBC_Rs.

Table 1

Primary Antibodies/lectin Used in This Study

Antigen	Dilution	Host, type	Source	Catalog no.	Immunogen
Calbindin	1:1000	Rabbit, polyclonal	Millipore (Billerica, MA)	AB1778	Recombinant mouse calbindin
GLT1A	1:500	Guinea pig polyclonal	LifeSpan Bioscience Inc (Seattle, WA)	LS-C15448	A synthetic peptide corresponding to amino acids 554-573 from the carboxy-terminus of rat GLT-1A
GLT1B	1:100	Mouse, monoclonal	Abcam plc (Cambridge, MA); Novus Biologicals, LLC (Littleton, CO)	Ab61859; NB110-58775	A synthetic peptide made to a C-terminal region within resides 548–562 of rat GLT1B.
Goα	1:500	Mouse, monoclonal	Chemicon International (Temecula, CA)	MAB3073	Purified bovine brain Goα
	1:200	Rabbit, polyclonal	Santa Cruz Biotechnology (Santa Cruz, CA)	Sc-387	A synthetic peptide corresponding to an internal region of Goα of rat origin
PKCα	1:1000	Rabbit, polyclonal	Sigma-Aldrich Co. LLC (St. Louis, MO)	P4334	synthetic peptide corresponding to amino acids 659–672 from the C-terminal variable (V5) region of rat PKCα
	1:250	Mouse, monoclonal	BD Transduction Lab. (San Jose, CA)	610107	Human PKCα aa. 270–427 Recombin a nt Protein
PSD95	1:100	Rabbit, polyclonal	Abcam plc (Cambridge, MA)	Ab18258	Synthetic peptide conjugated to KLH derived from within residues 50 – 150 of Mouse PSD95
Peanut agglutinin	1:50	-	Vector Laboratories Inc (Burlingame, CA)	FL-1071	-